Supporting information

Ligand-Length Engineering in Isoreticular Fe-MOFs Enables Efficient Ciprofloxacin Degradation

Hanqi Li,[†a] Xinyan Qiu,[†a] Shiyu Yuan, [a] Yanyi Lu,[a] Xiaoran Yan,[a] Yuzheng Guo,[c,d] Zhuo Jiang,[a,b*]

a. School of Electrical Engineering and Automation, Wuhan University, Wuhan 430072, China.
b. Shenzhen Research Institute of Wuhan University , shenzhen 518057, China.
c. School of Power and Mechanical Engineering, Wuhan University, Wuhan 430072, China.
d. Hubei Key Laboratory of Electronic Manufacturing and Packaging Integration, Wuhan University, Wuhan 430072, China.

† Hanqi Li and Xinyan Qiu contributed equally to this work.

*Corresponding author.

E-mail addresses: zhuojiang@whu.edu.cn (Z.Jiang), hanqili1206@whu.edu.cn (H. Li), qiuxinyan@whu.edu.cn (X. Qiu)

Table of Contents

Section S1. Material and Analytical methods

Material

Table S1.Chemicals

Reagent	Molecular Formula	Specification	Manufacturer
Hydrochloric acid	HCl	AR，36-38%	Sinopharm Chemical Reagent Co., Ltd.
Ethylenediamine tetraacetic acid disodium salt dihydrate	$C_{10}H_{14}N_2O_8Na_2 \cdot 2H_2O$	AR	Sinopharm Chemical Reagent Co., Ltd.
Iron(iii) chloride hexahydrate	$FeCl_3 \cdot 6H_2O$	ACS	Shanghai Aladdin Biochemical Technology Co., Ltd.
2,6-naphthalenedicarboxylic acid	$C_{12}H_8O_4$	≥98%(T)	Shanghai Aladdin Biochemical Technology Co., Ltd.
Ciprofloxacin	$C_{17}H_{18}FN_3O_3$	Biotechnology level，90%	Shanghai Yuanye Biotechnology Co., Ltd.
p-phthalic acid	$C_8H_6O_4$	99%	Shanghai Aladdin Biochemical Technology Co., Ltd.
Fumaric acid	$C_4H_4O_4$	>99.0%	Shanghai TCI Chemical Industry Development Co., Ltd.
Ethanol absolute	C_2H_5OH	AR	Sinopharm Chemical Reagent Co., Ltd.
Methanol	CH_3OH	AR	Sinopharm Chemical Reagent Co., Ltd.
Sodium hydroxide	NaOH	AR	Sinopharm Chemical Reagent Co., Ltd.
Iron(iii) nitrate nonahydrate	$Fe(NO_3)_3 \cdot 9H_2O$	AR	Shanghai Aladdin Biochemical Technology Co., Ltd.
N,N-dimethylformamide	C_3H_7NO	AR	Sinopharm Chemical Reagent Co., Ltd.
p-benzoquinone	$C_6H_4O_2$	HPLC	Shanghai Aladdin Biochemical Technology Co., Ltd.

Biphenyl-4,4'-dicarboxylic acid	$C_{14}H_{10}O_4$	≥97%	Shanghai Aladdin Biochemical Technology Co., Ltd.
Tert-butanol	$(CH_3)_3COH$	AR	Sinopharm Chemical Reagent Co., Ltd.
Hydrogen peroxide	H_2O_2	AR，30%	Sinopharm Chemical Reagent Co., Ltd.
Nitric acid	HNO_3	AR	Sinopharm Chemical Reagent Co., Ltd.

Ultrapure water was obtained from the lab-based ultrapure water system.

Analytical methods

The degradation efficiency of CIP is calculated according to the following formula:

$$\text{Degradation rate} = (C_0\text{-}C_t)/C_0 \times 100\%$$

where C_0 represents the concentration of CIP at -15 minutes, and C_t represents the concentration of CIP at t minutes.

Section S2. Characterizations

The crystal phase composition of MIL-88 series were characterized by using X-ray diffraction (XRD, Smartlab-9kW, Rigaku Japan) and scanning electron microscopy (SEM, Zeiss GeminiSEM 500, Britain, using voltage of 2 keV). Time-resolved fluorescence spectra were obtained on FLS1000 fluorescence lifetime spectrometer with 365-nm excitation light. The O^{2-}• and •OH produced by the photocatalyst were detected by the Electron paramagnetic resonance (EPR, EPR200M, China). The proportion of MOF added to the solution during the test was consistent with that of the experiment. The electronic state and coordination environment of survey spectrum and Fe 2*p* in the catalyst was characterized by X-ray photoelectron spectroscopy (XPS, ESCALAB Xi+, Thermo Fisher Scientific, America). N_2 adsorption isotherms were measured on iPore 400 instrument (PhysiChem Instruments Ltd). Before the N_2 adsorption measurements, all the samples were fully degassed by heating at 150 ℃ under vacuum for 8 h. A liquid nitrogen bath (77 K) was used for isotherm measurements. Ultra-high purity grade N_2 was used to the adsorption experiments. UV–vis diffuse reflectance spectra (DRS) were measured on a UV-VIS spectrophotometer UV-2600 (SHIMADZU). The flat-band potentials (E_{fb}) of samples were recorded on an electrochemical workstation (CHI 760E) in a typical three-electrode cell filled with 50 mL of a 0.5 M Na_2SO_4 solution. Pt and a saturated Ag/AgCl electrode were used as the counter electrode and the reference electrode, respectively. The working electrode was prepared by deposition 4 mg sample suspension on a fluorine-tin-oxide-coated (FTO coated) glass with area of 1 × 1 cm², followed by volatilization the solvent at room temperature. All spin-polarized density functional theory (DFT) calculations were performed using the Vienna Ab-initio Simulation Package (VASP)[1]. The exchange-correlation functional was treated with the generalized gradient approximation (GGA) in the Perdew-Burke-Ernzerhof (PBE) formulation[2]. The projector augmented wave (PAW) method was employed to describe ion-electron interactions. A plane-wave basis set was expanded with a kinetic energy cutoff of 520 eV. For the metal-organic framework system, a large periodic supercell was adopted. Due to the significant lattice dimensions, the Brillouin zone was sampled using a Γ-centered $2 \times 2 \times 1$ k-point mesh. The convergence criterion for electronic self-consistent field (SCF) cycles was set to 10^{-6} eV. All structures were fully relaxed until the residual interatomic forces were less than 0.02 eV/Å. The Grimme's dispersion correction scheme was employed to account for long-range van der Waals interactions[3], while the solvation effects were considered using the implicit solvent model, VASPsol[4].To further investigate the electronic properties, the band-decomposed charge densities of the valence band maximum (VBM) and conduction band minimum (CBM) were extracted using the VASPKIT package. This analysis provides a spatial visualization of the electronic states contributing to the band edges, facilitating an understanding of the charge localization and potential separation mechanisms between the Fe centers and the organic ligands.

Section S3. Statistical particle size distribution of the MIL-88 series

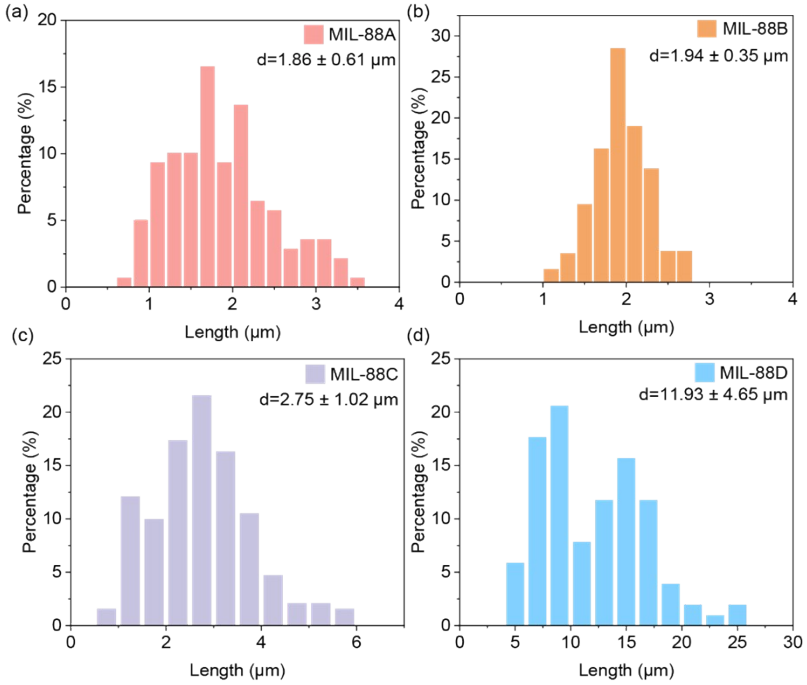

Figure S1. Statistical particle size (length) distribution plot of the MIL-88 series, derived from the statistics of Figure 2a-d.

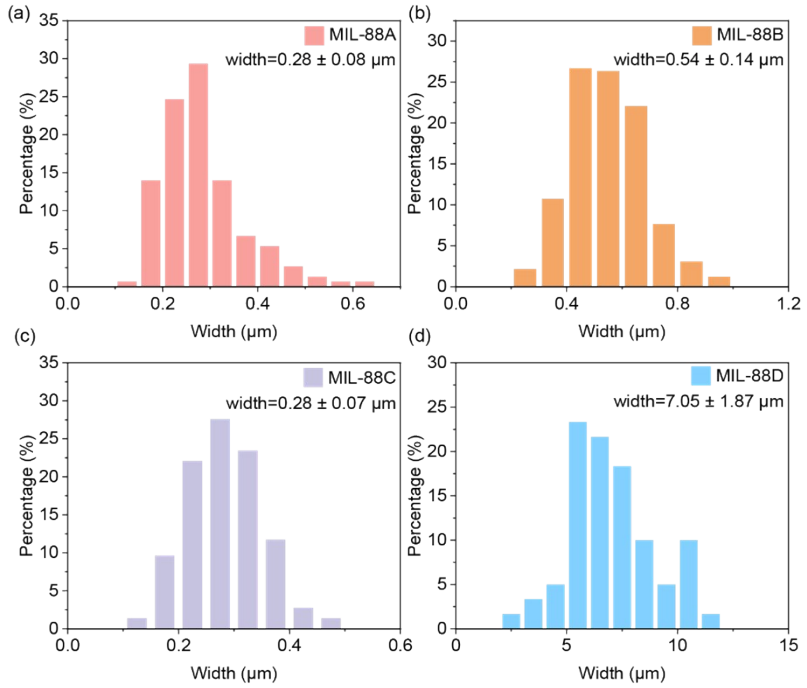

Figure S2. Statistical particle size (width) distribution plot of the MIL-88 series, derived from the statistics of Figure 2a-d.

Section S4. Diffuse Reflectance Spectroscopy (DRS) and Mott-Schottky test

The band gap of MIL-88-A, -B, -C, -D were derived from their diffuse reflectance spectroscopy (DRS) patterns (Figures 3d). The E_{fb} value of MIL-88-A, -B, -C, -D were calculated by using the Mott-Schottky relation formula:

$$C^{-2}=(2/\varepsilon\varepsilon_0 N_d)(V_a-E_{fb}-Kt/e)$$

where C is the space charge layer capacitance, e is the electron change, ε is the dielectric constant, ε_0 is the permittivity of vacuum, N_a is the electron donor density, and V_a is the applied potential. (Figures S1-S4)

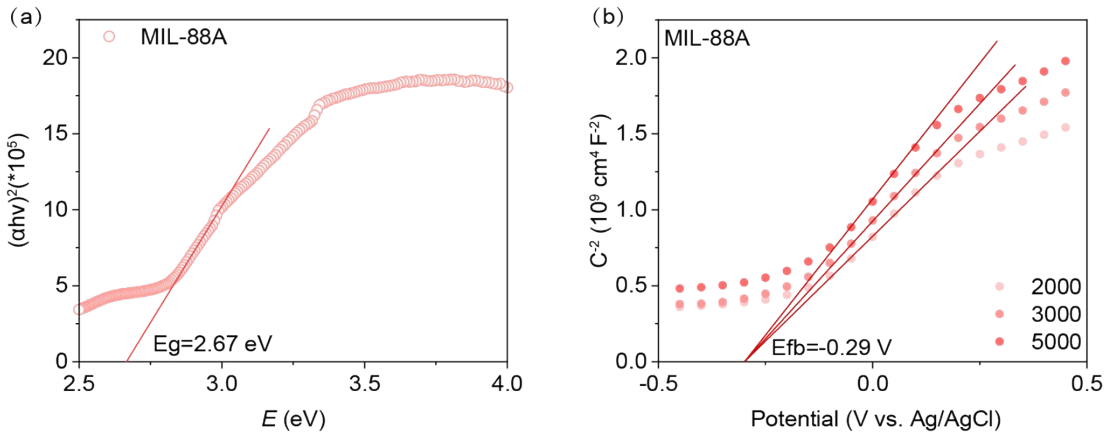

Figure S3. (a) Tauc plot, (b) Mott-Schottky measurement of MIL-88A.

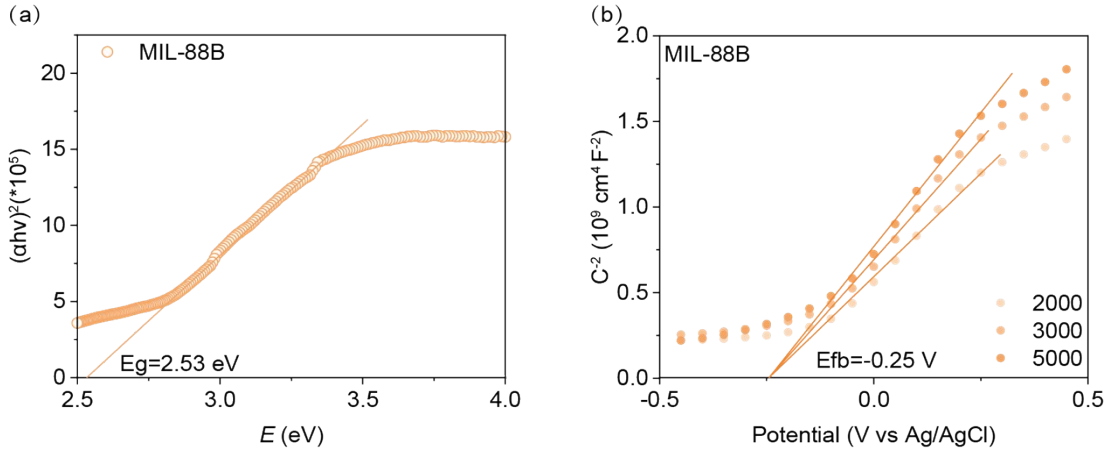

Figure S4. (a) Tauc plot, (b) Mott-Schottky measurement of MIL-88B.

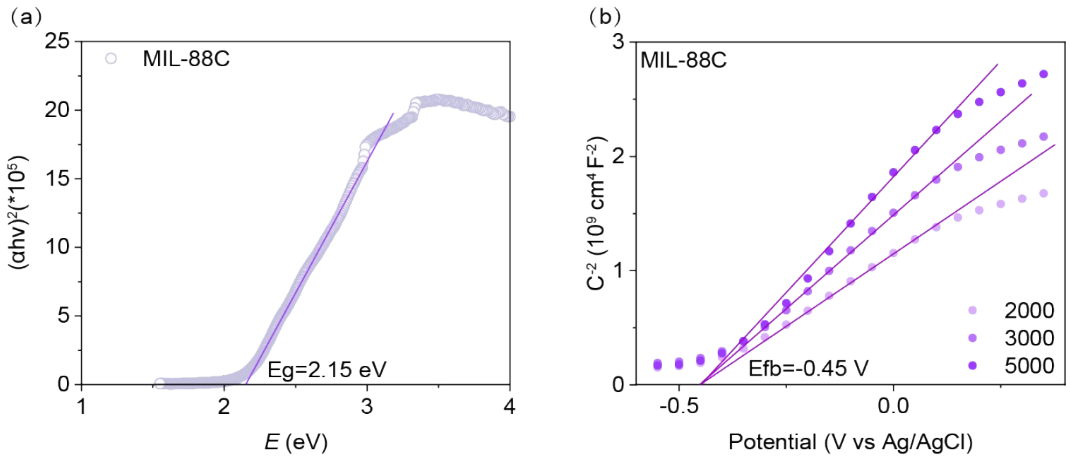

Figure S5. (a) Tauc plot, (b) Mott-Schottky measurement of MIL-88C.

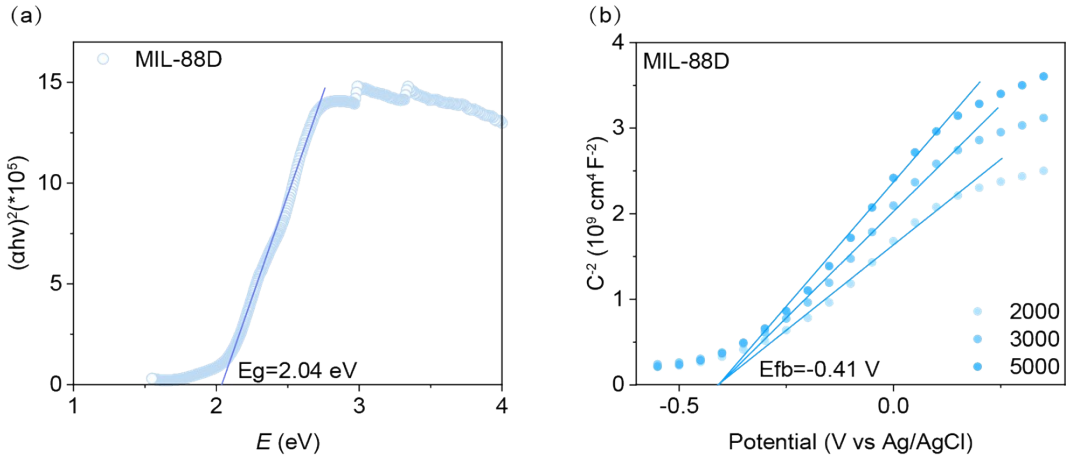

Figure S6. (a) Tauc plot, (b) Mott-Schottky measurement of MIL-88D.

Section S5. Photocatalytic degradation of the CIP series experiments

If no special instructions are given, the degradation CIP (25ppm, 100mL) experiments are generally conducted in visible light, pH=5, using H_2O_2 concentration is 1mL/L, and the catalyst mass was 0.1 g/L. The addition amount of the scavenger in the free radical quenching experiment was: BQ: p-benzoquinone, 0.5mM; TBA: tert-butanol, 5mM; MeOH: methanol, 10%vol

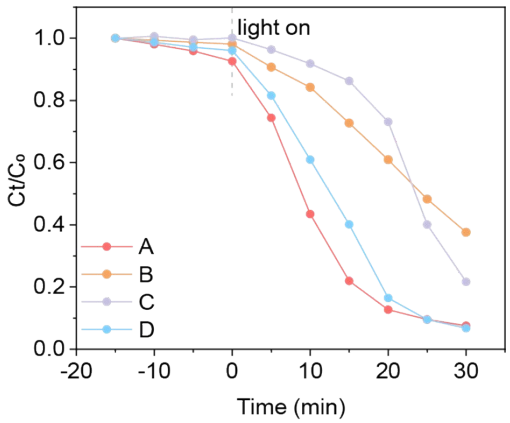

Figure S7. Degradation test of MIL-88-A, -B, -C, -D under the same conditions.

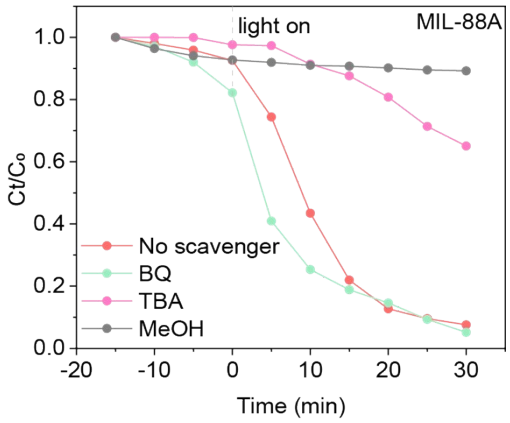

Figure S8. Free radical quenching experiments of MIL-88A with different scavengers.

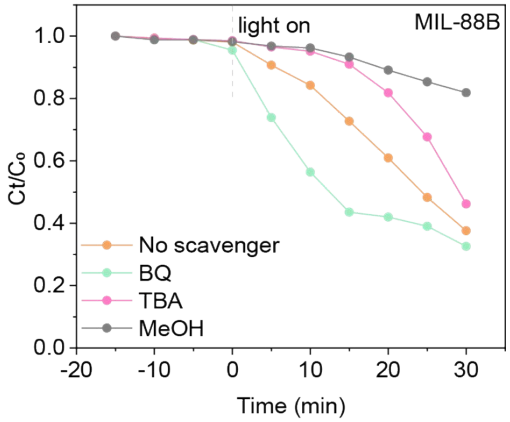

Figure S9. Free radical quenching experiments of MIL-88B with different scavengers.

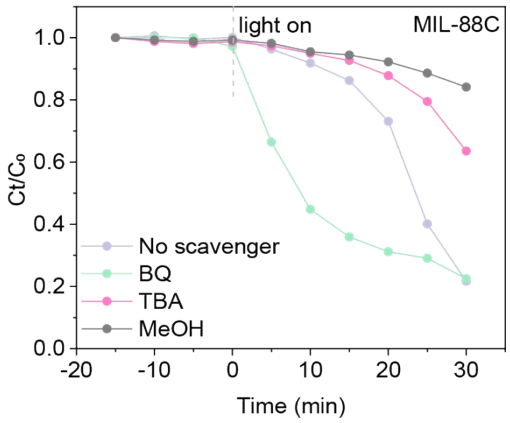

Figure S10. Free radical quenching experiments of MIL-88C with different scavengers.

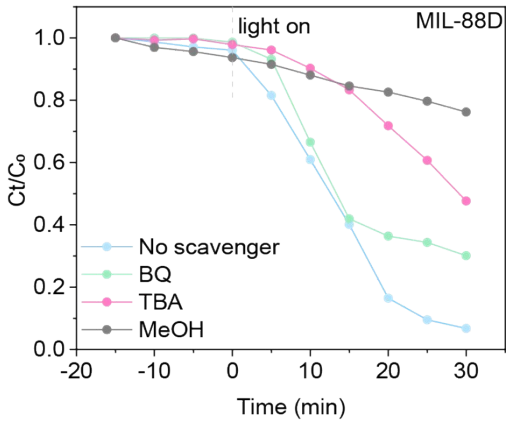

Figure S11. Free radical quenching experiments of MIL-88D with different scavengers.

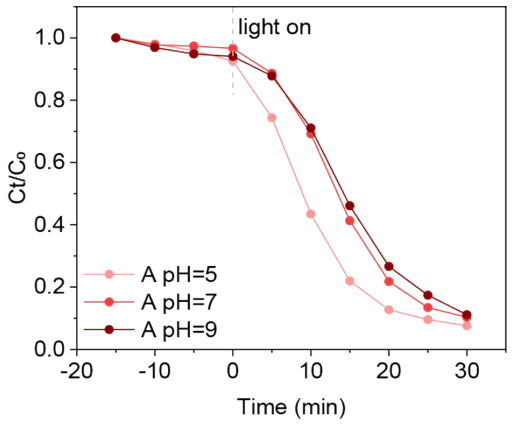

Figure S12. Photocatalytic degradation of MIL-88A at different pH conditions.

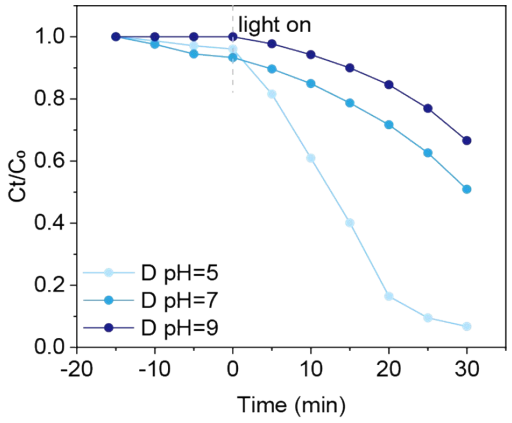

Figure S13. Photocatalytic degradation of MIL-88D at different pH conditions.

Section S6. XRD pattern before and after catalysis

As shown in Figure S14, the characteristic diffraction peaks of both MIL-88A and MIL-88D remain well preserved after the catalytic reaction, with no noticeable shift in peak positions. This indicates that the crystalline frameworks of both MOFs are well maintained without structural degradation during the reaction. It is worth noting that a slight change in the relative peak intensity within the 10°-12.5° range is observed for MIL-88A after catalysis. This variation can be attributed to incomplete dehydration of the framework, which leads to a breathing effect commonly observed in MOF materials[5].

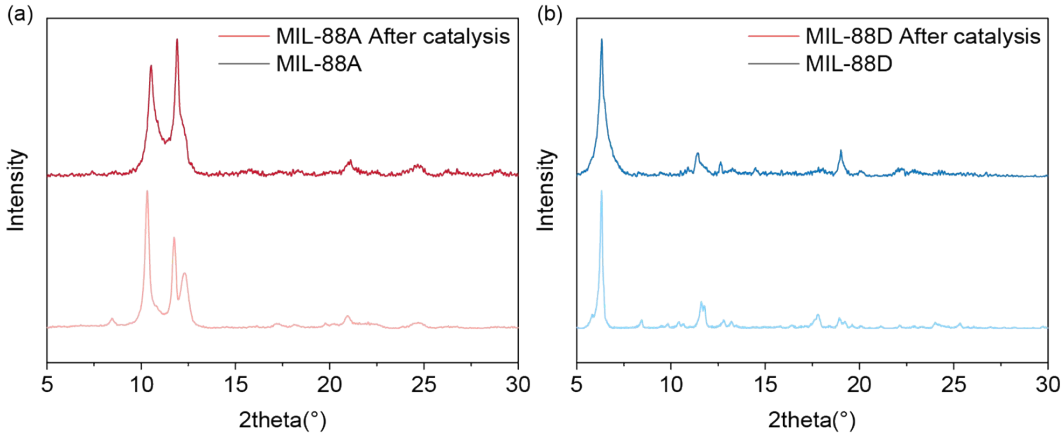

Figure S14 XRD of MIL-88A (a) and MIL-88D (b) before and after catalysis

Section S7.TC-HCl degradation experiment

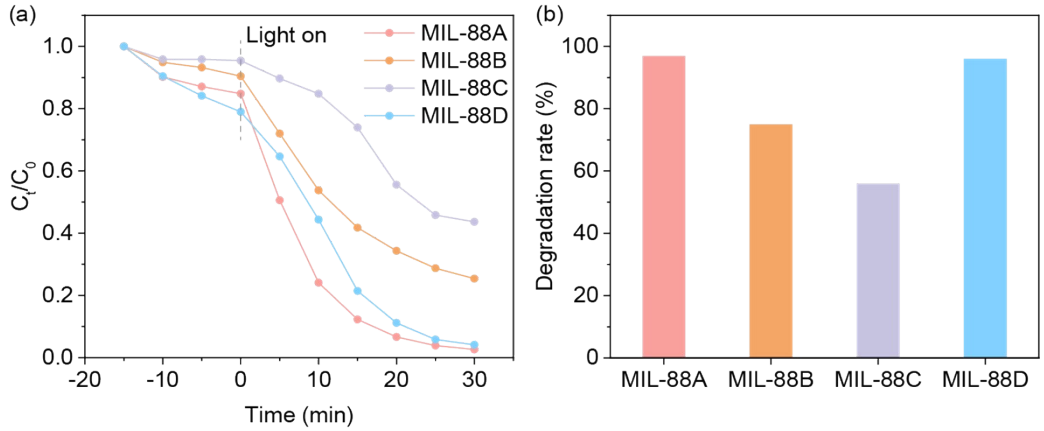

Figure S15. (a) Degradation profiles and (b) degradation efficiencies of the MIL-88 series catalysts toward 25 ppm TC-HCl.The catalyst dosage, solution pH, and H_2O_2 amount were kept consistent with those used in the CIP degradation experiments.

Section S8. Kinetic fitting of CIP degradation

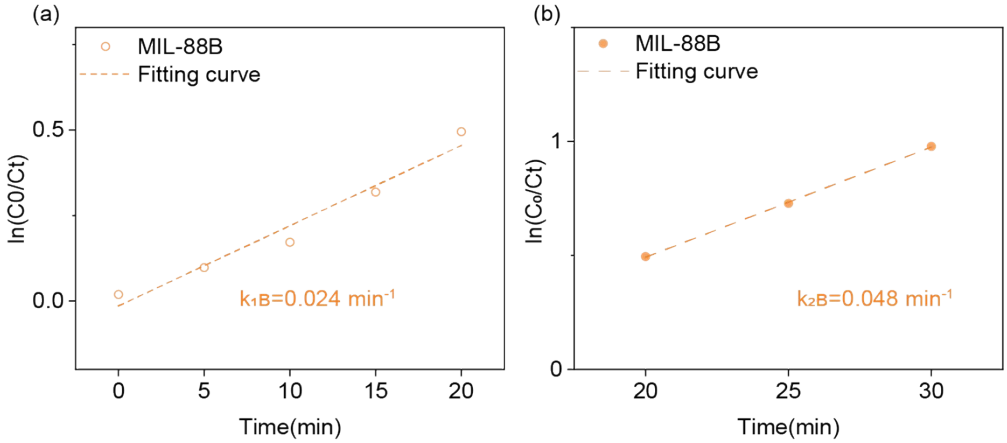

Figure S16. Kinetic fitting of MIL-88B (a)in the first 20 minutes; (b) after 20 minutes.

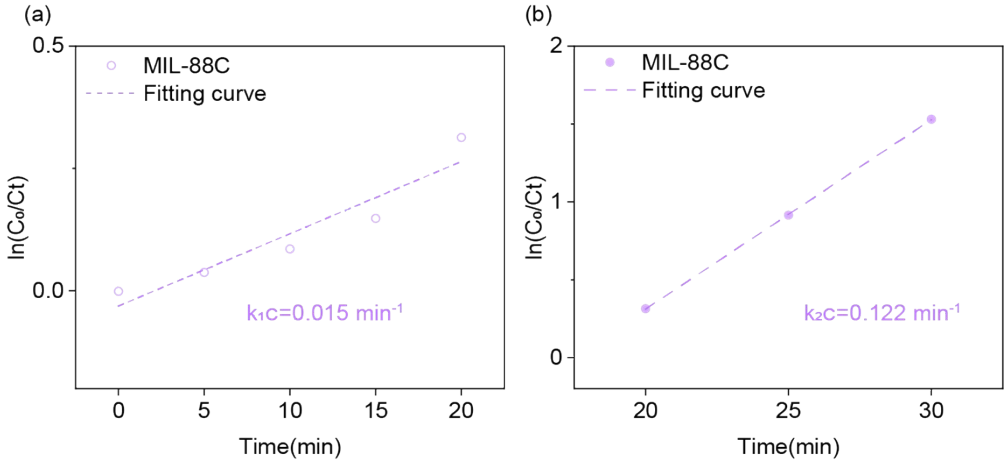

Figure S17. Kinetic fitting of MIL-88C (a)in the first 20 minutes; (b) after 20 minutes.

Table S2. Kinetic fitting constants for the degradation of CIP over time

	MIL-88A	MIL-88B	MIL-88C	MIL-88D
$k_1(min^{-1})$	0.104	0.026	0.015	0.058
$k_2(min^{-1})$	0.052	0.048	0.122	0.118

Section S9. Degradation experiments at low CIP concentration

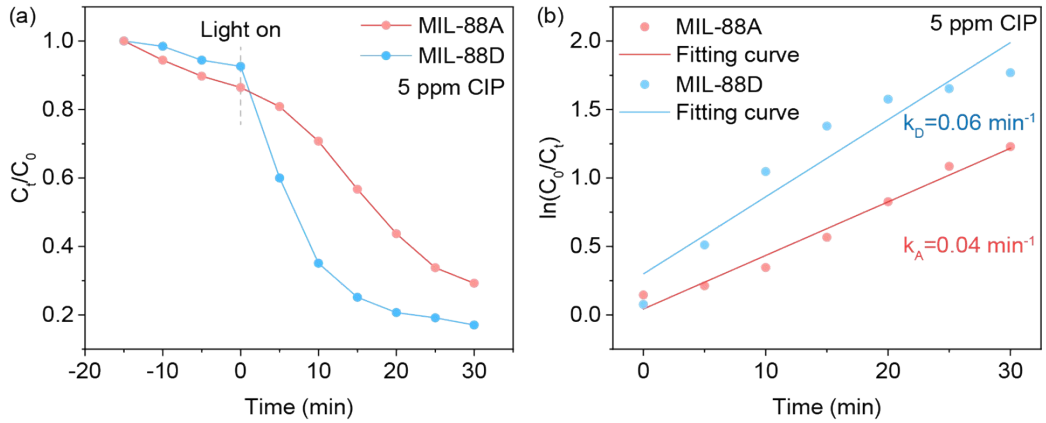

Figure S18. (a) Degradation experiments of MIL-88A and MIL-88D at 5 ppm and (b) Kinetic fitting.

Section S10. Measured DMPO-trapped Electron paramagnetic resonance (EPR) signals

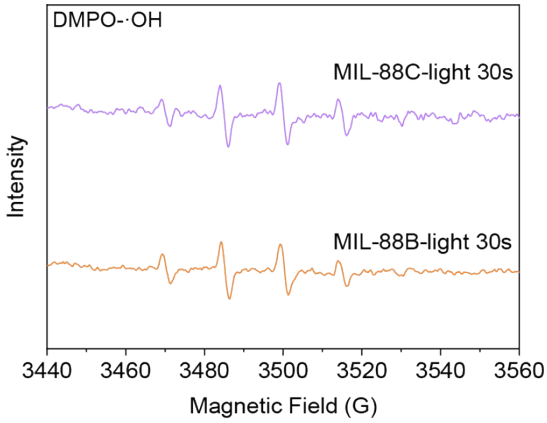

Figure S19. ·OH radical trapping experiment of MIL-88B and MIL-88C under illumination.

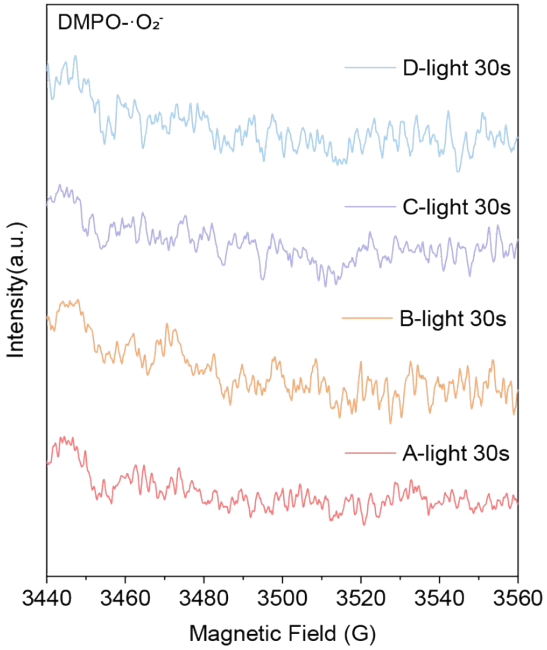

Figure S20. $\cdot O_2^-$ radical trapping experiment of MIL-88A, B, C, D under illumination.

Section S11. N_2 adsorption analysis

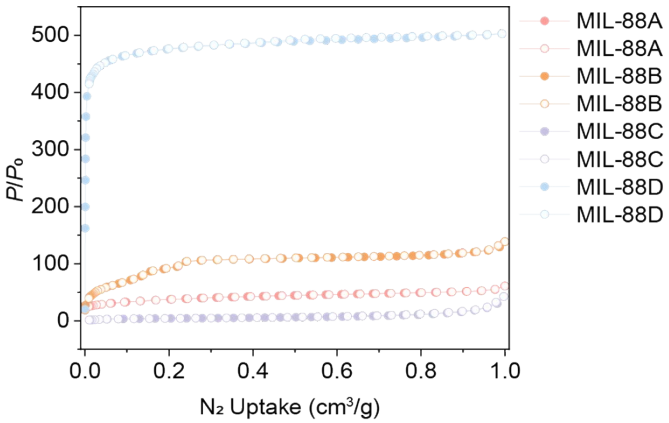

Figure S21. N_2 adsorption analysis of MIL-88A, B, C, D

Section S12. Normalized the catalytic activity by the specific surface area

Table S3. MIL-88 Series normalized the catalytic activity by the specific surface area

	MIL-88A	MIL-88B	MIL-88C	MIL-88D
TON(h^{-1})	401.07	271.12	341.12	406.37
BET surface area(m^2/g)	131.81	359.96	15.12	1914.71
TON / BET surface area	3.04	0.75	22.56	0.21

Section S13. The fluorescence lifetime, photocurrent and valence band spectrum of MIL-88-B, -C

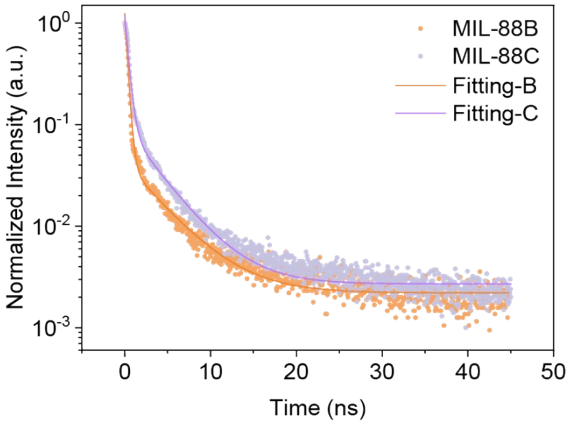

Figure S22. Transient fluorescence decay curves received at 480nm under excitation light of 365nm for MIL-88B and MIL-88C.

Table S4. Transient fluorescence lifetime fitting results

	MIL-88A	MIL-88B	MIL-88C	MIL-88D
A_1	97%	96%	93%	85%
τ_1(ns)	0.27	0.30	0.41	0.63
A_2	3%	4%	7%	14%
τ_2(ns)	4.03	4.32	3.78	4.63
τ_{ave}(ns)	1.19	1.62	1.90	2.84

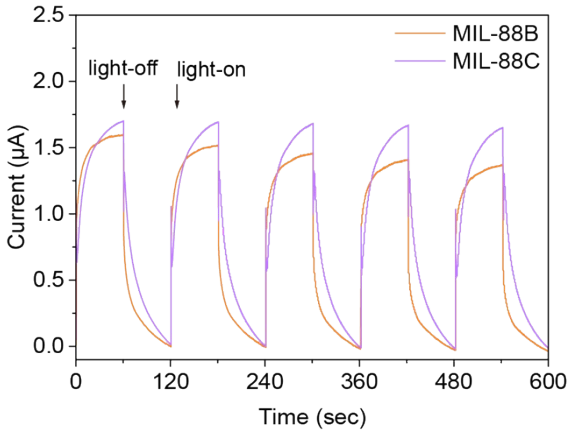

Figure S23. Transient photocurrent responses of MIL-88B and MIL-88C.

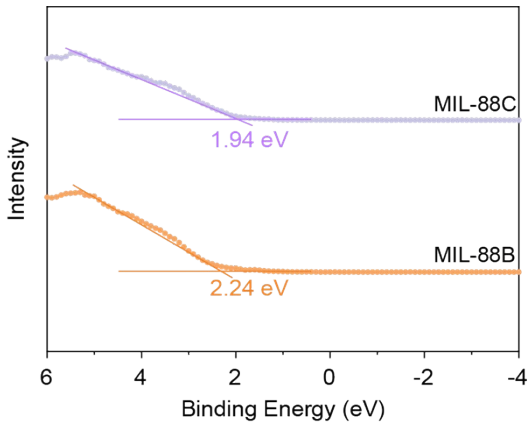

Figure S24. Valence band spectra of MIL-88A and MIL-88D

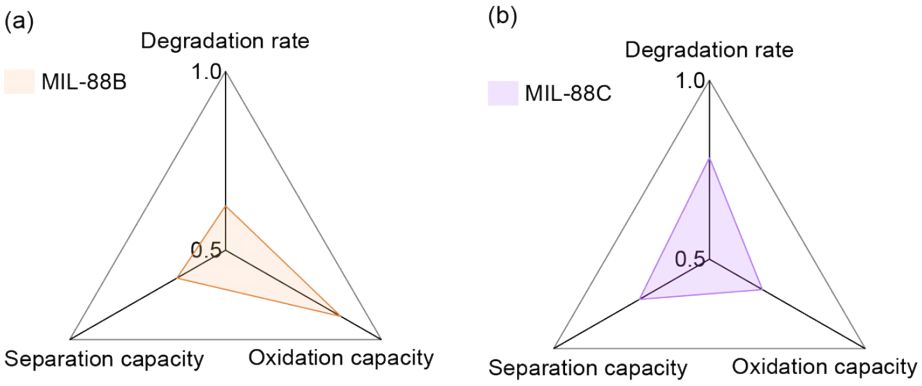

Figure S25. Shows the radar charts based on degradation efficiency, separation efficiency, and oxidation capacity (a) MIL-88B, (b) MIL-88C

Section S14. In-situ light-induced XPS

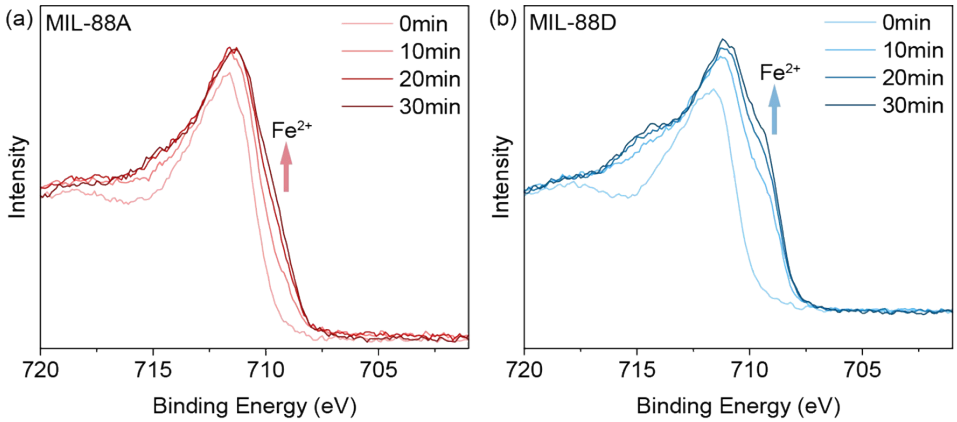

Figure S26. In-situ light-induced XPS of (a)MIL-88A; (b)MIL-88D.

Section S15. Performance comparison of Fe-MOF in photocatalytic degradation of CIP

Table S5. Performance comparison of Fe-MOF in photocatalytic degradation of CIP

MOF	Light	pH	Degradation performance at 30 minutes	Ref.
MIL-88A	Visible light	5	92.44%	This work
MIL-88D	Visible light	5	93.25%	This work
MIL-88B	Visible light	5	62.38%	This work
MIL-88C	Visible light	5	78.35%	This work
NH_2-MIL-101	Visible light	7	10.36%	6
MIL-53(Fe-Cu)	Visible light	4	34.23%	7
Fe-BDC	Xenon lamp	7	33.32%	8
MIL-100(Fe)	Visible light	6.96	15.81%	9
UiO-66-on-MIL-101(Fe)/WA	Ultraviolet lamp	7	54.03%	10
UiO-66-on-MIL-101(Fe)/WA	Ultraviolet lamp	7	18.57%	11
Fe-TCPP-3	Visible light	7	73.00%	12
MIL-53(Fe)-NH_2	Visible light	7	43.69%	13
ZIF-67 @ MIL-100(Fe)	Xenon lamp	4.3	49.40%	14

References

1. G. Kresse and J. Furthmüller, *Computational Materials Science*, 1996, **6**, 15-50.
2. J. P. Perdew, K. Burke and M. Ernzerhof, *Physical Review Letters*, 1996, **77**, 3865-3868.
3. S. Grimme, *Journal of Computational Chemistry*, 2006, **27**, 1787-1799.
4. K. Mathew, R. Sundararaman, K. Letchworth-Weaver, T. A. Arias and R. G. Hennig, *The Journal of Chemical Physics*, 2014, **140**, 084106.
5. C. Serre, C. Mellot-Draznieks, S. Surblé, N. Audebrand, Y. Filinchuk and G. Férey, *Science*, 2007, **315**, 1828-1831.
6. N. Kaushal, A. A. Taha, S. Tyagi and P. G. Smirniotis, *Mater. Chem. Phys.*, 2025, **332**, 130198.
7. A. Chatterjee, A. K. Jana and J. K. Basu, *New J. Chem.*, 2021, **45**, 17196-17210.
8. V. T. Le, V. A. Tran, D. L. Tran, T. L. H. Nguyen and V.-D. Doan, *Chemosphere*, 2021, **270**, 129417.
9. W.-Q. Li, Y.-X. Wang, J.-Q. Chen, N.-N. Hou, Y.-M. Li, X.-C. Liu, R.-R. Ding, G.-N. Zhou, Q. Li, X.-G. Zhou and Y. Mu, *Appl. Catal. B-Environ. Energy*, 2022, **302**, 120882.
10. Li, X. Zhang, X. Huang, X. Li, Q. Chang, S. Deng and G. Zhu, *J. Water Process. Eng.*, 2024, **63**, 105442.
11. P. Yang, C. Y. Hu, Z. W. Jiang, S. Y. Xiao, X. Y. Wang, C. Z. Huang, Y. F. Li and S. J. Zhen, *J. Colloid Interface Sci.*, 2022, **622**, 690-699.
12. H. Haitosa, L. He, P. Chen, D. M. Kabtamu, O. A. Zelekew and Y.-n. Wu, *J. Environ. Chem. Eng.*, 2025, **13**, 120296.
13. He, M. Lv, H. Dong, Q. Chen, M. Hassan, J. Niu and Z. Gong, *Sep. Purif. Technol.*, 2024, **340**, 126645.